

Article

Effect of Biogenic Silica Behavior in the Incorporation of Mesoporous Anatase TiO₂ for Excellent Photocatalytic Mineralization of Sodium Diclofenac

Christian Brice Dantio Nguela ^{1,2}, Ngomo Horace Manga ¹, Clément Marchal ² , Aimé Victoire Abega ^{2,3}, Ndi Julius Nsami ¹ and Didier Robert ^{2,*} 

¹ Laboratory of Applied Physical and Analytical Chemistry, Department of Inorganic Chemistry, Faculty of Science, University of Yaounde1, Yaoundé P.O. Box 812, Cameroon

² Institut de Chimie et Procédés pour l'Énergie, l'Environnement et la Santé, UMR-CNRS 7515, Université de Strasbourg, 25 rue Becquerel, 67087 Strasbourg, France

³ Department of Chemistry, Faculty of Sciences, University of Douala, Douala P.O. Box 24157, Cameroon

* Correspondence: didier.robert@univ-lorraine.fr

Abstract: TiO₂/SiO₂ composites were synthesized via a simple sol gel method by surface reduction of Ti⁴⁺ ions to Ti³⁺ using titanium isopropoxide as a TiO₂ precursor and rice husks (RHA) as a SiO₂ source. The silica content and calcination temperature of the materials were evaluated. Thermal, crystallographic and physicochemical aspects suggest that biogenic silica (SiO₂) can improve the thermal stability of the anatase phase of TiO₂, when the SiO₂ content reaches 20%. The N₂ adsorption-desorption isotherms showed that the SiO₂-modified samples have uniform pore diameters and a large specific surface area. The XPS analysis showed the surface reduction of Ti⁴⁺ ions to Ti³⁺ within the TiO₂ network via oxygen vacancies after SiO₂ introduction, which is beneficial for the photocatalytic reaction. Photocatalytic degradation of sodium diclofenac (SDFC) shows that TiO₂/SiO₂ composites have better activity compared to commercial P25. Mesoporous TiO₂ composite modified with 20 wt% SiO₂ showed better photocatalytic mineralization than P25 (83.7% after 2 h instead of 57.3% for P25). The excellent photocatalytic mineralization of the photocatalysts can be attributed to the high anatase crystallinity exhibited by XRD analysis, high specific surface area, surface hydroxyl groups, and the creation of oxygen vacancy, as well as the presence of Ti³⁺ ions.

Keywords: biogenic silica; TiO₂ anatase; photocatalysis; mineralization; sodium diclofenac



Citation: Dantio Nguela, C.B.; Manga, N.H.; Marchal, C.; Abega, A.V.; Nsami, N.J.; Robert, D. Effect of Biogenic Silica Behavior in the Incorporation of Mesoporous Anatase TiO₂ for Excellent Photocatalytic Mineralization of Sodium Diclofenac. *Catalysts* **2022**, *12*, 1001. <https://doi.org/10.3390/catal12091001>

Academic Editor: Simonetta Palmas

Received: 5 August 2022

Accepted: 30 August 2022

Published: 5 September 2022

Publisher's Note: MDPI stays neutral with regard to jurisdictional claims in published maps and institutional affiliations.



Copyright: © 2022 by the authors. Licensee MDPI, Basel, Switzerland. This article is an open access article distributed under the terms and conditions of the Creative Commons Attribution (CC BY) license (<https://creativecommons.org/licenses/by/4.0/>).

1. Introduction

Pharmaceuticals and personal care products (PPCPs) present in wastewater have potential negative impacts on humans and ecosystems, even when present in trace amounts [1]. Among these contaminants, sodium diclofenac (SDCF) is a non-steroidal anti-inflammatory drug commonly used as an analgesic, anti-arthritic, and anti-rheumatic drug [2]. Its biodegradation and natural attenuation are quite limited [3]. Among the different processes implemented for the removal of SDCF, heterogeneous photocatalysis is considered an effective method to achieve its mineralization [4,5]. During the last two decades, heterogeneous photocatalysis has been demonstrated to be a “green” and effective method for water purification and disinfection [6]. This process is based on the absorption of light by a semiconductor, usually TiO₂, to produce electron–hole pairs, reacting at the interface to produce oxidizing species such as hydroxyl or superoxide radical. One of the main advantages of photocatalysis is the capacity to mineralize, without selectivity, the majority of organic compounds.

TiO₂ is one of the most widely used photocatalysts, due to its high activity, chemical stability, low toxicity, strong oxidizing power to decompose organic pollutants, and environmental friendliness [7]. It has been widely studied for water purification, hydrogen

production, self-cleaning surfaces, etc. [8]. However, TiO₂ anatase powders, although having high surface areas, are not stable at high temperatures and easily lose their quantum efficiency and adsorption capacity, by phase transformation and crystallite growth [9], which considerably limits their photocatalytic efficiency [10]. Recently, our research group synthesized the carbon nanotube/TiO₂ composite nanomaterial in which Ti³⁺ ions and oxygen vacancies appeared within the TiO₂ band gap as a sub-band (sub-level). This composite showed a consistent improvement in the degradation of methyl orange under visible light irradiation [11]. Another strategy to solve this problem is to combine TiO₂ with SiO₂ [12,13]. SiO₂ is a very important inorganic material used for a wide range of commercial applications such as molecular sieves, catalysts, and in biomedical and electrical applications. Biogenic SiO₂ has been studied as potential support due to its high specific surface area, porous structure, thermal stability, ability to effectively decrease aggregation, and transparency in the UV light range [14–16]. This biogenic silica could be a by-product of rice production, especially rice husks, with a relative humidity of approximately 20–25% by weight of the total dry weight of the rice [16,17]. According to Ndindeng et al., there are 5 million tons of rice produced per year by sub-Saharan African countries, leading to high waste rice husks discharged into the environment [18]. Due to its low mechanical strength, low nutritional value and low bulk density, its use is limited [19]. However, rice husks contain a large amount of silica, approximately 98% of the total inorganic compounds [20], which can be used as raw material to produce value-added silicon-based materials with interesting texture and morphology. The implementation of such substances from rice husks is very interesting for the fact that they come from biomass, which is a renewable energy source [21]. Over the past decade, this area of research has progressed considerably and expanded, driven by the global emphasis on sustainable and renewable resources. As a chemically inert material, porous silica plays an important role in various applications, including in adsorption and as catalyst support. It can be artificially synthesized with a certain degree of control in its nano-morphology [22], and this usually involves a complicated process. Most of the time, a large amount of amorphous silica is produced by multi-step thermal reduction of raw silica at high temperatures and high pressures under extremely acidic and energy-intensive conditions, which have a high impact on the environment [18]. Therefore, it is important to develop an affordable, sustainable, and environmentally friendly technique for the manufacture of porous silica to meet the growing demand for its widespread applications. Until now, many works have been interested in the synthesis of TiO₂/SiO₂ composites with different methods such as thermal and solvothermal hydrolysis [23], the sol-gel method [24], the hydrothermal method [25], and spray coating [26]. However, most of these methods use tetraethyl orthosilicate (TEOS) as a silica precursor and require several steps in the syntheses, high temperatures and pressures, and are also expensive.

The present work is based on the synthesis of TiO₂ nanoparticles homogeneously and uniformly dispersed on the surface of biogenic silica nanoparticles by a simple sol-gel method, in which the surface reduction of Ti⁴⁺ ions to Ti³⁺ occurred to generate electronic states below the conduction band of TiO₂. The Ti³⁺ ions act as a sub-band gap to reduce the recombination rate of photogenerated electrons/holes pairs. The nanomaterials were characterized using thermogravimetric analysis, X-ray diffraction (XRD), scanning electron microscopy (SEM), UV-Vis diffuse reflectance spectroscopy, X-ray photoelectron spectroscopy (XPS), Brunauer–Emmett–Teller Analysis (BET), Fourier transform infrared (FT-IR), and energy dispersive X-ray analysis (EDX). The photocatalytic performance of the synthesized nanomaterials on the degradation of sodium diclofenac as a model pollutant in an aqueous solution under UV-A irradiation is also reported.

2. Results and Discussion

2.1. Thermal Analysis

Thermogravimetric (TG) and differential scanning calorimetric (DSC) analysis data of TiO₂ gels prepared without SiO₂ and with 20% SiO₂ are shown in Figure 1. The DSC curve shows that the TG exhibit three similar thermal accidents, although they are different from each other in terms of weight changes. The first loss at approximately 100 °C corresponds to the removal of adsorbed water, on pure TiO₂ and the 20% T/S composite, respectively. The second loss with a large exothermic peak at 245 °C corresponds to the partial elimination of hydroxyl groups. It can be seen that the weight loss of T/S 20% is higher than that of TiO₂. This may be due to the presence of more hydroxyl groups introduced by SiO₂ that are easier to eliminate at 245 °C [27]. Finally, the last loss corresponds to the transformation of amorphous TiO₂ to crystalline TiO₂ anatase observed at 381.8 °C for pure TiO₂ and increases to 386.1 °C for the T/S 20% composite in agreement with the X-ray diffraction results (see next section).

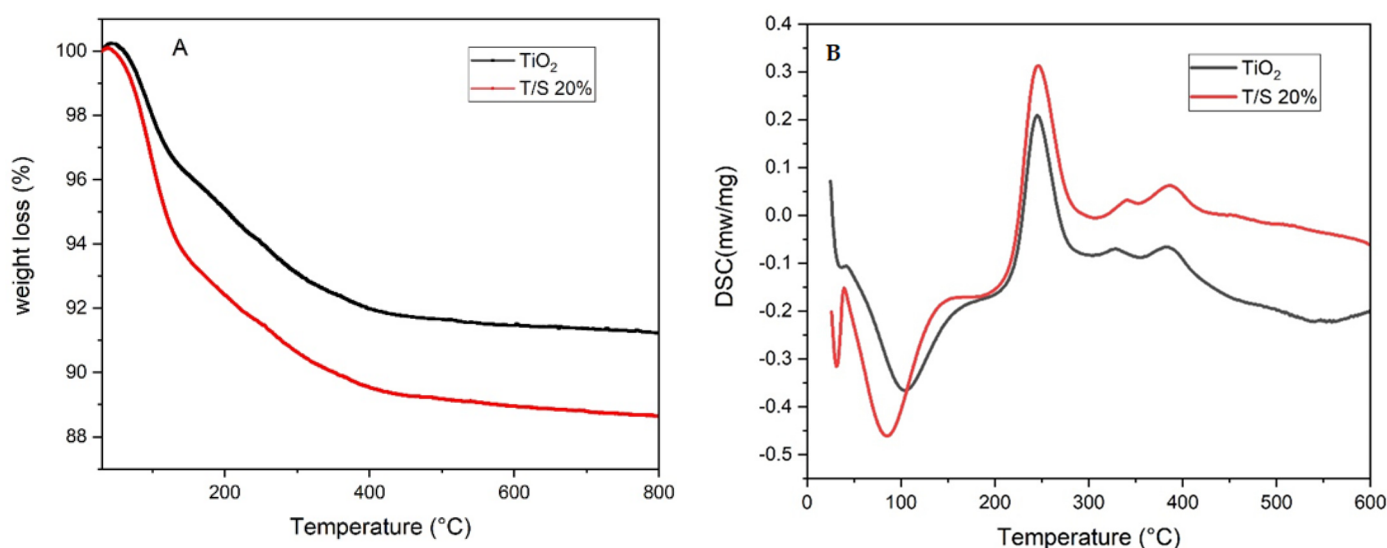


Figure 1. ATG (A) and DSC (B) curves of pure TiO₂ and 20% T/S composite.

2.2. Structural Analysis

It can be seen (Figure 2A) that the silica nanoparticles show an amorphous phase with a wide diffraction peak between 15 and 30°, which is in good agreement with the literature [20]. The DRX pattern of pure TiO₂ shows the presence of anatase and rutile phases for TiO₂ calcined at 650 °C. The diffraction peaks at 25.3°, 38.83°, 48.11°, 53.95°, 62.79°, 69.0°, and 70.46° correspond to the (101), (004), (200), (211), (204), (220), and (215) planes of the anatase, respectively (ICSD:033547). The diffraction peaks at 27.54°, 36.17°, 39.28°, 41.32°, 44.14°, 54.54°, 56.66°, 64.15°, and 69.0° correspond to the (110), (101), (200), (111), (211), (220), (002), (310), and (301) planes of the rutile, respectively. The diagram of TiO₂/SiO₂ composites shows that silica nanoparticles play a major role in the thermal stability of pure TiO₂. When the silica content is less or equal to 5%, a weak rutile phase peak is observed, which disappears by increasing the silica content to 20%. This shows that silica can delay the transformation of the anatase phase to rutile and reduce the size of TiO₂ crystallites (Figure 3). The decrease in crystallite size can be attributed to the good dispersion of TiO₂ on the silica surface, which prevents any possible agglomeration of the nanoparticles [28].

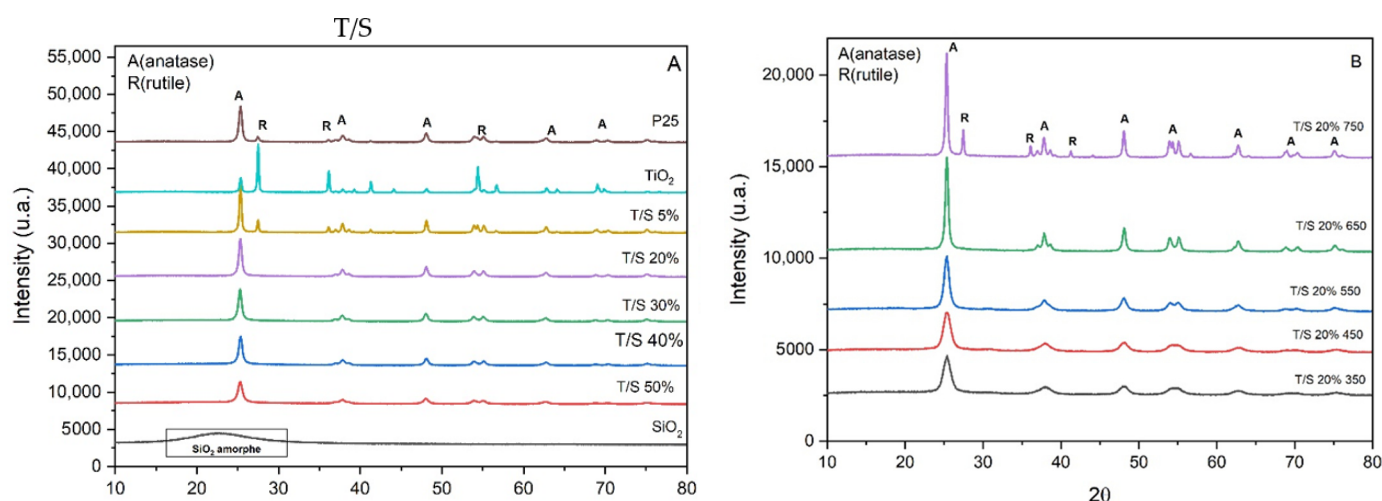


Figure 2. X-ray diffractogram of samples (A): SiO₂, T/S–X at 650 °C (B): TS 20%–T.

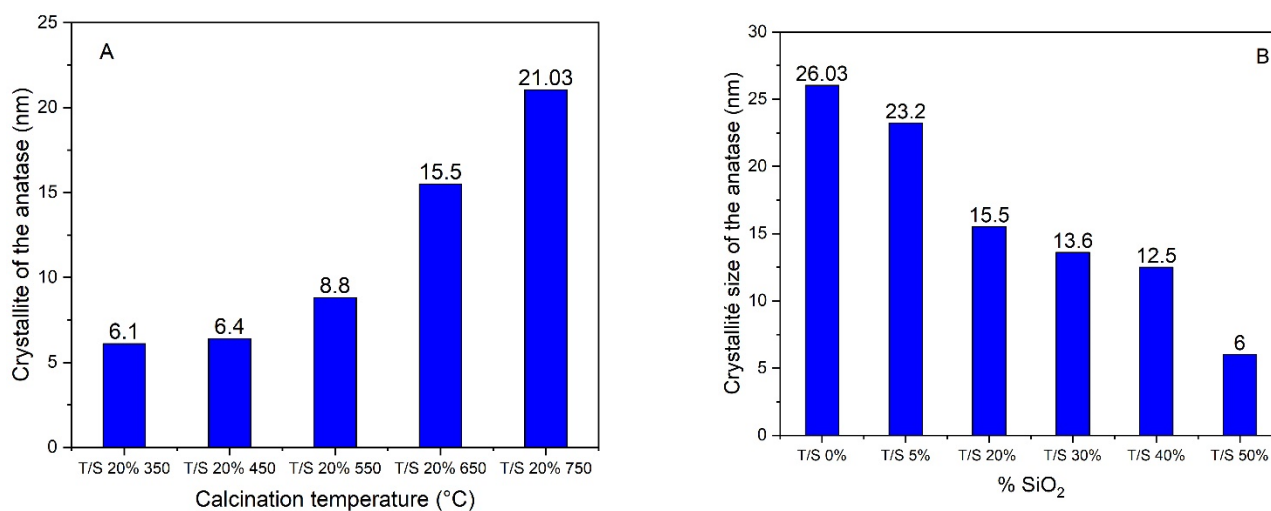


Figure 3. Anatase crystallite sizes of samples (A): T/S 20%–T (T = Temperature); (B): T/S–X (X = wt% SiO₂) calcined at 650 °C.

In Figure 2B, it can be seen that the main phase of the T/S 20% composite calcined at 350 °C is pure anatase. When the temperature increases, the anatase peaks become progressively strong and narrow, and the anatase crystallite size increases from 6.1 nm to 21.03 nm at 750 °C (Figure 3) with the appearance of rutile peaks. This is confirmed by a change in lattice parameters ‘a’ and ‘c’ of the composites (Table 1), causing a decrease in microstrain and dislocation density as the temperature increases. This implies that the transition temperature of the anatase to rutile is between 650 and 750 °C. The microstrains (δ) and dislocation density (ϵ) were obtained by Equations (1) and (2), while the average crystallite size (D) of the anatase nanoparticles was obtained by the Debye–Scherrer equation (Equation (3)) using the peak attributed to the anatase crystal planes (101) by the following relations:

$$D = \frac{k\lambda}{\beta \cos\theta} \quad (1)$$

$$\epsilon = \frac{\beta}{4 \tan\theta} \quad (2)$$

$$\delta = \frac{1}{D^2} \quad (3)$$

where λ is the X-ray wavelength, θ is a specific angle, β is the width at half maximum (FWHM) for the anatase peak (101), and k is the constant depending on the shape of the crystallites (k is 0.9 when the particles are spherical).

Table 1. Crystallographic parameters of the synthesized materials.

Samples	2θ (°)	a = b	c	c/a Ratio	Anatase Nanoparticles Size (nm)	Microstrain $\times 10^{-3}$	Dislocation Density $\times 10^{-3}$
T/S 20% 450	25.37	3.7850	9.5140	2.514	6.37	23.97	24.61
T/S 20% 550	25.32	3.7858	9.5074	2.511	8.85	17.35	12.78
T/S 20% 650	25.34	3.7842	9.5146	2.514	15.48	9.90	4.17
T/S 20% 750	25.31	3.7850	9.5140	2.514	21.03	7.31	2.26
TiO ₂ pur 650	25.35	3.7850	9.5140	2.514	26.03	5.88	1.48

The results in Table 1 and Figure 2 clearly show that the average crystallite size increases with temperature and decreases with silica content. This clearly indicates that the presence of SiO₂ allows good dispersion of TiO₂ particles on its surface (see SEM in Section SEM and EDX Analysis), thus giving photocatalytic nanomaterials with a large specific surface area.

2.3. Mesoporous Structure

Figure 4 shows the adsorption–desorption isotherms of N₂ for SiO₂, TiO₂, and T/S-X calcinated at 650 °C. The type IV isotherms show an H₃-type hysteresis loop corresponding to capillary condensation on the mesopores. This confirms the mesoporous characteristic of the materials, which possesses significant importance in the adsorption of organic molecules. Furthermore, this result suggests that SiO₂ effectively preserves the TiO₂ mesostructures, especially when SiO₂ content reaches 20%. Moreover, the pore volume increases with the SiO₂ content of composite materials, whereas the pore diameter decreases. These results suggest an increase in surface availability of the target pollutant, leading to an improvement in adsorption capacity. The effect of silica on the specific surface area shows that the surface area of the photocatalysts composite increases with SiO₂ content, which further demonstrates the importance of SiO₂ in TiO₂ dispersion (Table 2).

SEM and EDX Analysis

It can be seen in Figure 5 that SiO₂ is similar to highly porous cloud-like platelets stacked more or less densely (Figure 5A). Figure 5B shows that pure TiO₂ shows obvious agglomerated particles with denser and larger particles, which leads to a decrease in surface area in agreement with the BET result. In contrast, the 20% T/S composite has a relatively uniform TiO₂ nanoparticle distribution with less aggregation and a porous microstructure (Figure 5C). This material exhibits the characteristics of a large 2D porous plate covered with a small bead. It is noted that said platelets are bonded in-plane with a strong decrease in platelet stacking. This result indicates that silica can improve the regularity of mesopores, inhibiting the growth of nanocrystallites and agglomeration of TiO₂ nanoparticles. The chemical composition of T/S20% was determined by EDX analysis (Figure 5D). The results show that the main elements on its surface area are O, Si, and Ti. The Si element confirms the existence of SiO₂ in the structure of TiO₂. The mass percentages of the different elements are 37%, 1.5%, and 61.5%, respectively, in the composite (see composition in Figure 5D) for the elements O, Si, and Ti.

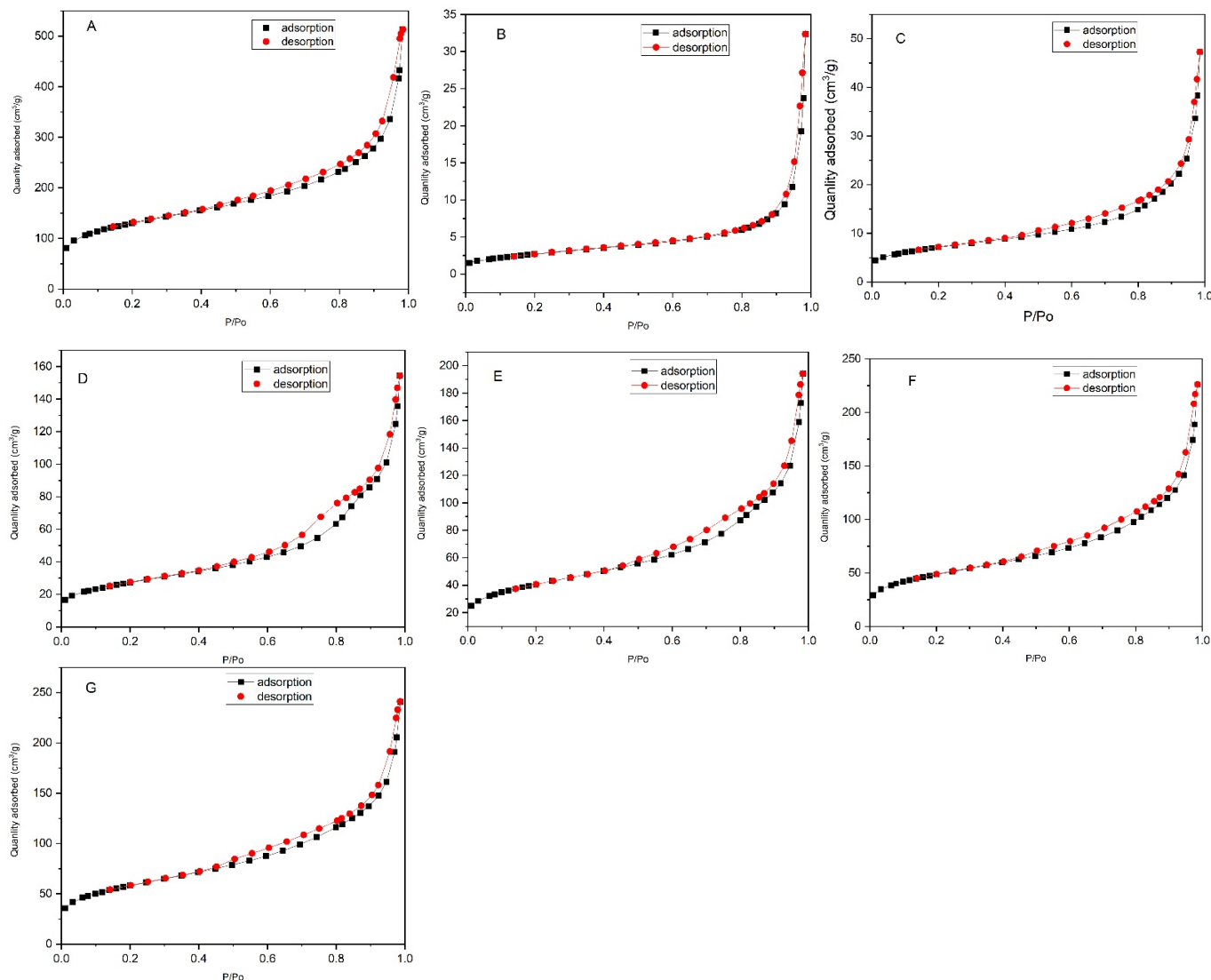


Figure 4. Nitrogen adsorption–desorption isotherm curves for (A) SiO₂, (B) TiO₂, (C) T/S 5%, (D) T/S 20%, (E) T/S 30%, (F) T/S 40%, (G) T/S 50%.

Table 2. Effect of silica on the specific surface area (S_{BET}) of materials compared to pure TiO₂.

Samples	SiO ₂	TiO ₂	T/S5%	T/S 20%	T/S 30%	T/S 40%	T/S 50%
specific surface area (m ² /g)	455.22	8.99	25.41	97.72	144.29	171.75	205.69
Pores volume (cm ³ /g)	0.718	0.047	0.071	0.23	0.29	0.33	0.35
Pores diameter (nm)	9.64	24.112	13.89	11.19	9.99	10.03	8.94

2.4. Surface Property

The IR spectrum of SiO₂ is given in Figure 6A, and the bands at 1063 and 799 cm^{−1} correspond to the characteristic asymmetric and symmetric stretching vibrations of the Si-O-Si bond, respectively. The bands at 958 and 450 cm^{−1} are attributed to the stretching vibrations of Si-O-H and Si-O bonds, while the bands at 1632 and 3414 cm^{−1} correspond, respectively, to the bending vibration of the Si-O-Si bond and stretching vibrations of the O-H bond adsorbed water [29].

Comparing the IR spectrum (Figure 6A) of SiO₂ to the IR spectra (Figure 6B,C) of samples with different SiO₂ contents and varying the calcination temperature, a weak band at approximately 3650 cm^{−1} is observed, which corresponds to the O-H bonds of the

coordination water. The broad bands at approximately 1630 and 3400 cm^{-1} correspond to the deformation and stretching vibrations, respectively, of the O-H bond of adsorbed, bound, or free water. The characteristic bands at 2985 and 2894 cm^{-1} correspond to the stretching vibrations of the $-\text{CH}_2$ bond. The bands at approximately 1070 cm^{-1} are attributed to the asymmetric vibration of Si-O-Si bonds in SiO_2 [30]. It can be noted that the number of hydroxyl bonds and the surface Si-O-Si bonds increases as the SiO_2 content increases (Figure 6B), and the O-H bonds in the T/S 20% sample remain constant until the calcination temperature reaches $650\text{ }^\circ\text{C}$. These results suggest that silica can effectively limit the loss of surface hydroxyl groups during calcination, thus the hydroxyl groups on the surface of the samples can be preserved, which is beneficial for the photocatalytic reaction in that these groups can increase molecule adsorption via coulombic attractions. This can be confirmed by the band at approximately 3400 cm^{-1} , which becomes broader. The decrease in the intensity of hydroxyl groups with increasing temperature (Figure 6C), can be caused by the aggregation of TiO_2 nanoparticles, which release the surface hydroxyl groups from SiO_2 and then become easily volatile at this temperature, according to the DRX analysis.

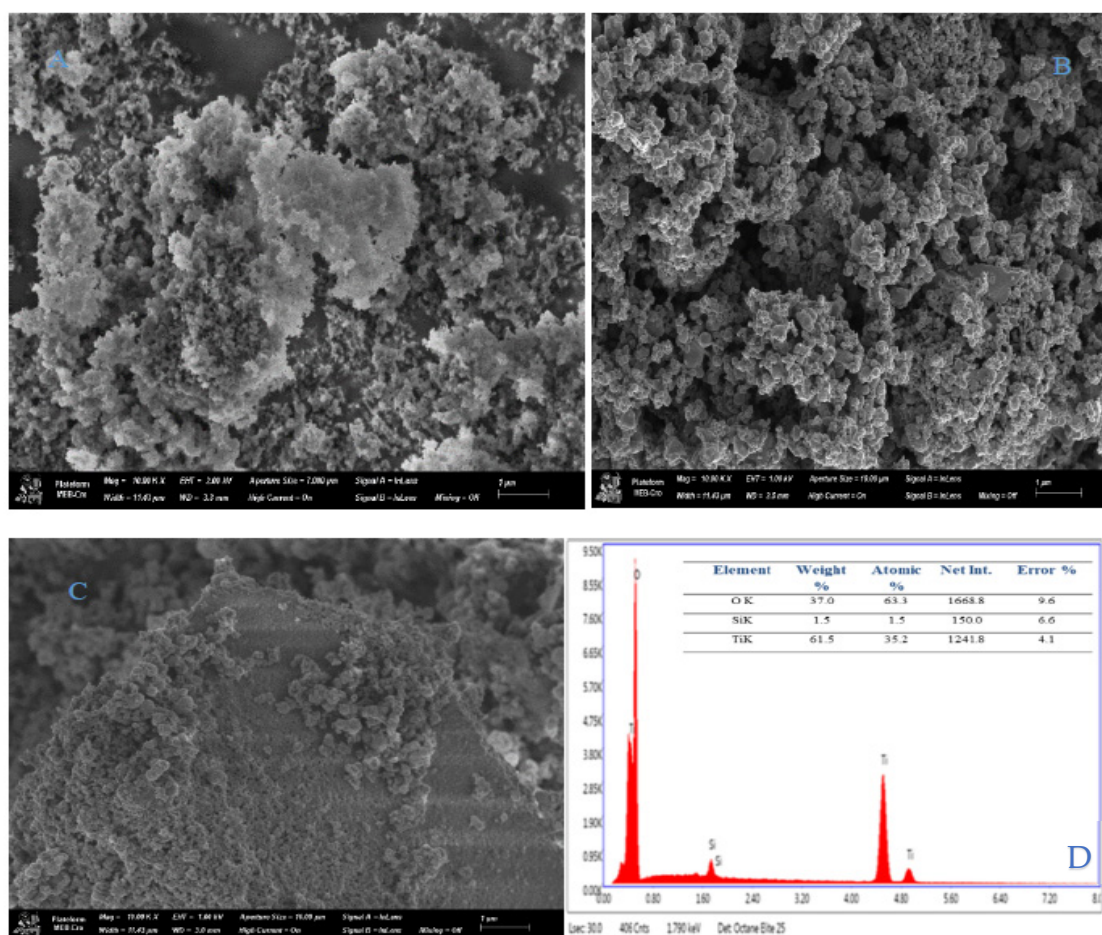


Figure 5. Scanning electron microscopy (SEM) of (A) SiO_2 , (B) TiO_2 , (C) T/S 20%, and (D) EDX-T/S 20%.

2.5. Surface Composition and Element Surface Oxidation State Analysis

To determine the surface composition as well as the oxidation state of the constituent elements of each material, XPS analysis was performed. This analysis clarified the existence, or not, of the Ti-O-Si bond in the SiO_2 -modified TiO_2 mesoporous. The XPS analysis of the T/S 20% composite calcined at $650\text{ }^\circ\text{C}$ (Figure 7A) shows the presence of three main peaks,

notably Ti 2p (456.33 eV), O 1s (528.84 eV), and Si 2p (102.84 eV), confirming that the TiO₂ nanoparticles are well coated on the surface of the silica nanoparticles.

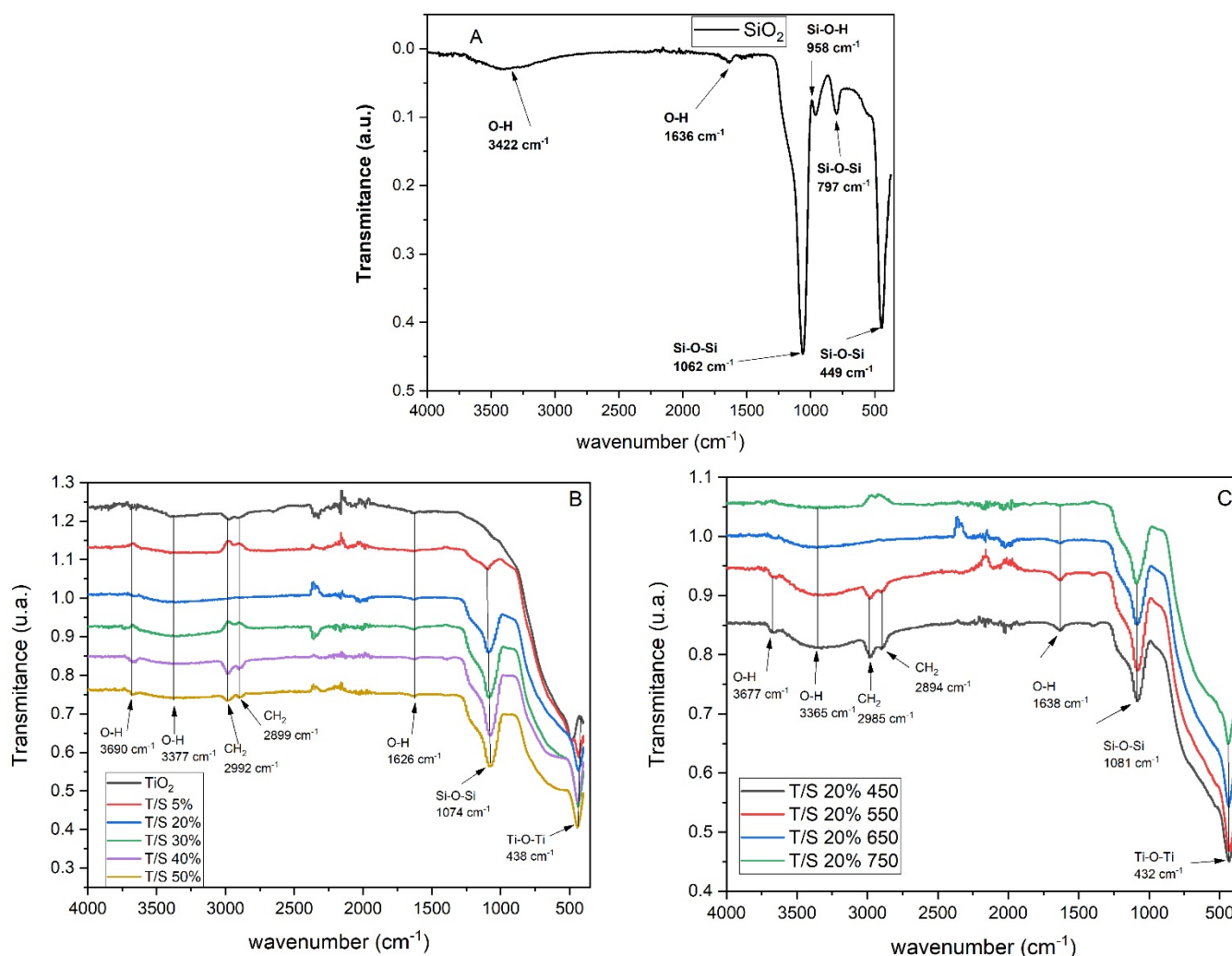


Figure 6. IR spectrum of (A) silica, the composites (B) T/S–X; (C) T/S–20%–T.

Figure 7B shows the deconvolution of the Ti 2p region, where the bands centered at 463.50 and 458.00 eV are assigned to Ti⁴⁺ 2p_{1/2} and Ti⁴⁺ 2p_{3/2}, respectively. On the other hand, the peaks at 461.03 and 455.50 eV are attributed to Ti³⁺ 2p_{1/2} and Ti³⁺ 2p_{3/2}, respectively, which may illustrate that Ti³⁺ ions are introduced due to the surface reduction of Ti⁴⁺ ions in the TiO₂/SiO₂ composite at high temperatures. Figure 7C shows the deconvolution of the O 1s peak, which can be divided into four peaks at 533.52, 531.00, 529.54, and 526.50 eV, which correspond to Si–O–Si, Ti–OH, and O₂^{2−} (O–Ti–O) bonds and oxygen vacancies, respectively. On this last point, it should be noted that with the increase in temperature, vacancies were created within TiO₂ according to the following equation:

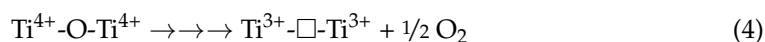


Figure 7D displays the Si 2p peak observed at 103.4 eV, indicating the existence of Si–O–Si bonding in the composite. Therefore, the results obtained from the XPS spectra are consistent with the infrared spectroscopy analysis.

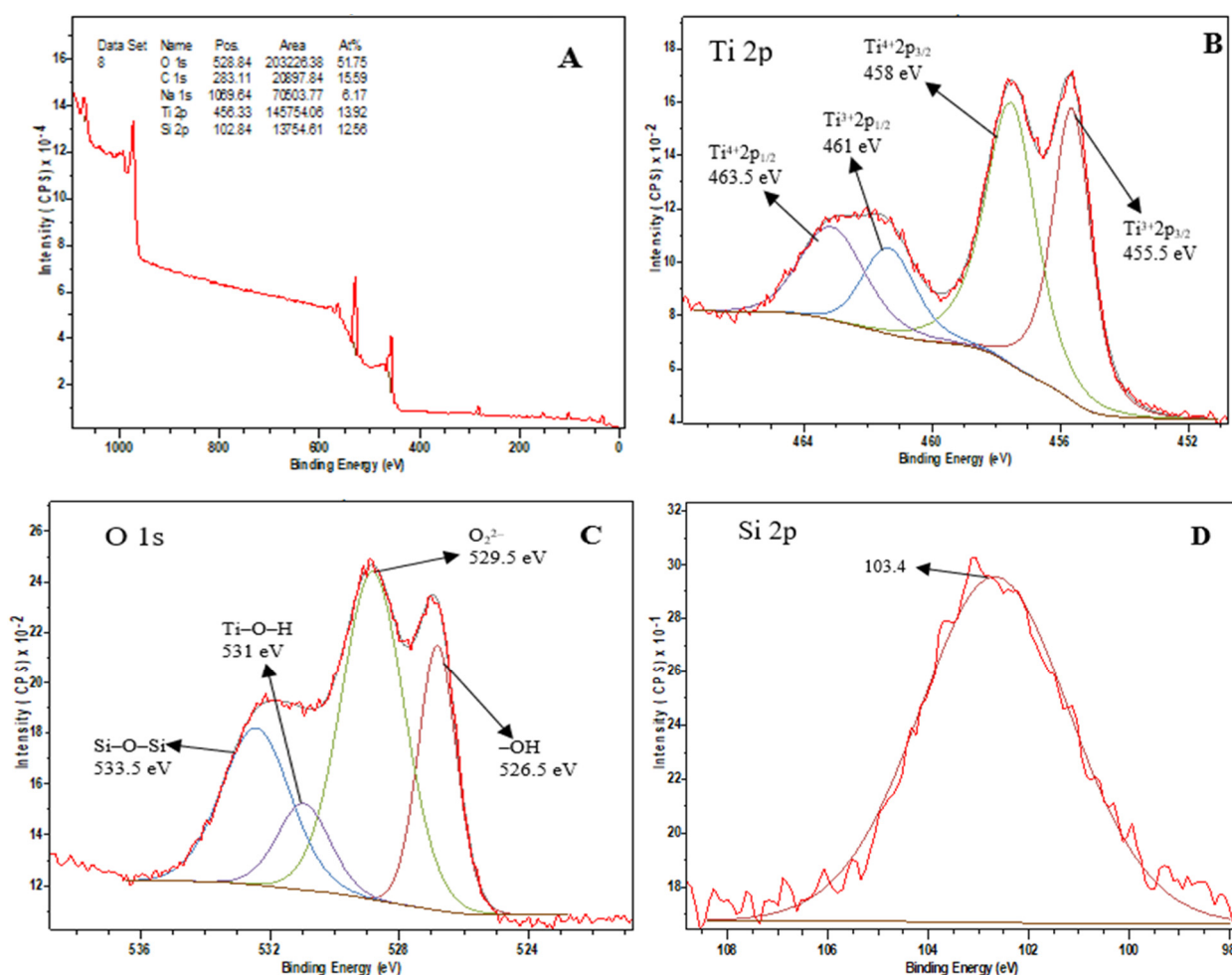


Figure 7. XPS spectrum of T/S 20% (A), Ti 2p (B), O 1s (C), and Si 2p (D) composites.

2.6. Photocatalytic Test for SDCF Mineralization

The photocatalytic efficiency of $\text{TiO}_2/\text{SiO}_2$ composites, $\text{TiO}_2\text{-P25}$, and pure TiO_2 was evaluated by degradation and mineralization of sodium diclofenac in an aqueous solution under UV-A radiation (60 W/m^2 , $\lambda_{\text{max}} = 368 \text{ nm}$). It can be seen from Figure 8A that the composite containing 20% of SiO_2 shows higher photocatalytic activity and also better mineralization than $\text{TiO}_2\text{-P25}$ (83.68% mineralization efficiency while $\text{TiO}_2\text{-P25}$ has only 57.33% after 120 min). These results reveal that silica can effectively enhance the photocatalytic activity of TiO_2 even at high temperatures. It can be seen that the calcination temperature has a significant effect on photocatalytic activity. As the calcination temperature increases up to $650 \text{ }^\circ\text{C}$, the 20% T/S composite always shows better photocatalytic activity and photocatalytic mineralization (Figure 8C) due to its large surface area, high crystallinity, and the presence of abundant hydroxyl groups on its surface. After calcination at $750 \text{ }^\circ\text{C}$, the photocatalytic activity decreases considerably due to the appearance of the rutile phase which is less active than the anatase phase. On the other hand, the increase in the size of the TiO_2 nanoparticles leads to a decrease in the surface contact with the pollutant and surface hydroxyl groups, which causes a decrease in the interactions with the target molecule. However, it still shows better photocatalytic mineralization than $\text{TiO}_2\text{-P25}$, with 74.56% mineralization after 120 min.

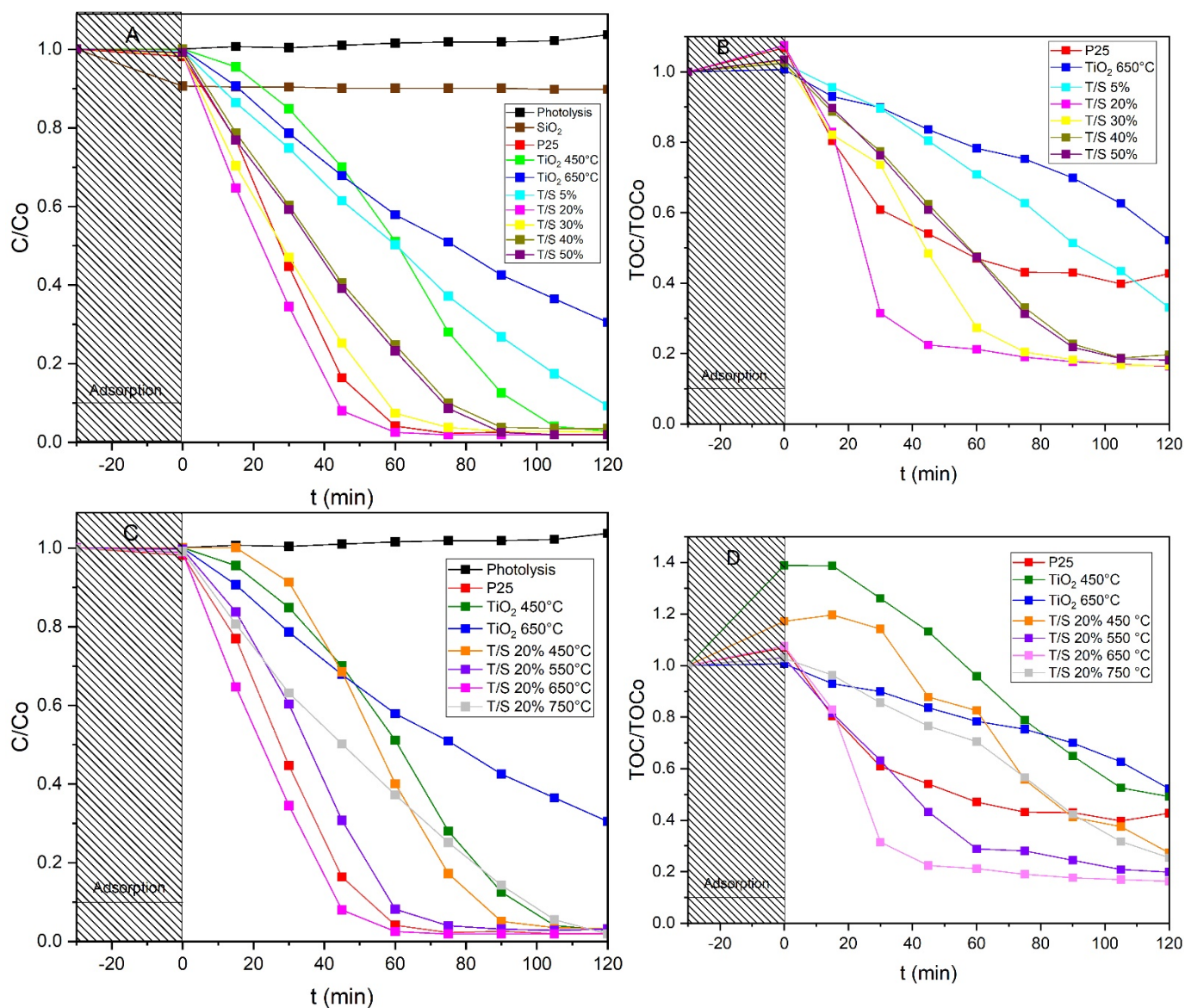


Figure 8. Photocatalytic degradation mineralization of SDCF in the presence of catalysts with different SiO_2 content compared to pure TiO_2 and commercial P25 (A,B) and in the presence of TS 20%–T catalyst calcined at different temperatures compared to pure TiO_2 and commercial P25 (C,D).

Good photocatalytic efficiency of the $\text{TiO}_2/\text{SiO}_2$ composites can be attributed to several factors. First, the size of the TiO_2 nanoparticles within the composites was smaller than that of pure TiO_2 calcined at 650°C . The decrease in particle size can shorten the time for the electron/hole pairs to reach the sample surface, which effectively reduces recombination charges and increases the rate of reduction or oxidation, thus improving the overall photocatalytic performance of the composite nanomaterial [31]. In addition, the absence of the rutile phase in the composite at 650°C promotes high photocatalytic activity.

Second, it is well known that the photocatalytic reaction is a surface reaction; thus, a large surface area is generally beneficial for photocatalytic reactions as it can provide more adsorption sites and photocatalytic reaction centers [16].

Third, TiO_2 combined with SiO_2 could effectively retain its mesoporous structure even at high calcination temperatures, which promotes the good diffusion of organic molecules into its structure, and results in high photocatalytic activity. Moreover, it has been reported that organic molecules have easier adsorption on the surface of TiO_2 in the presence of silica [32].

Finally, the composites have more surface hydroxyl groups compared to pure TiO₂ as FTIR analysis confirmed (see Section 2.4). It is widely believed that surface hydroxyl groups can capture photo-induced holes and produce active hydroxyl radicals and prevent electron–hole recombination at the same time [16].

3. Materials and Methods

3.1. Materials

All reagents used were of analytical grade and used without further purification: Titanetetraisopropoxide Ti(OC₃H₇)₄ (Aldrich, 97%), ethanol (SdS-France, 99.9%), H₂SO₄ (prolabo, 98%), NaOH (prolabo 98%), HCl (Prolabo, 37%), sodium Diclofenac (Aldrich 98%), and TiO₂-P25 (average size 20 nm, purity 97%, surface area 50 m²·g⁻¹ and 80% anatase, 20% rutile, Evonik industries). The rice husk samples used in this study were collected in the northwest Cameroon region in the locality of Ndop (6°00'00" North, 10°25'00" East), more precisely in the Ngo-ketunjia department.

3.2. Extraction of Nanosilica from Rice Husks

First, 150 g of rice husks previously washed with distilled water were refluxed with 500 mL (0.5 M) HCl at 70 °C for 2 h to remove metal impurities. After the complete reaction, the rice husks were washed several times with distilled water to remove HCl, and dried at 110 °C for 24 h. Then, the treated rice husks were calcinated at 800 °C with a heating rate of 10 °C/min for 2 h, to remove the carbonaceous material. White ash (silica) of high purity was obtained. The resulting ash was magnetically stirred with a 250 mL solution of 1 M NaOH for 2 h and filtered. The obtained solution was neutralized with 0.5 M sulfuric acid until the pH was equal to 2, after which a nanosilica gel was formed. This gel was then washed with distilled water until pH 7 was reached and then dried in an oven at 70 °C for 48 h to form a silica nanoparticle powder as shown in the following reactions:



Synthesis of TiO₂/SiO₂ Nanophotocatalysts

TiO₂/SiO₂ composites were synthesized using the sol-gel method for the reaction between titanium dioxide and silica. First, 15 mL of anhydrous ethanol was mixed with a certain amount of nanosilica (solution A). Meanwhile, 5 mL of Ti(OC₃H₇)₄ was dissolved in 15 mL of anhydrous ethanol and 30 mL of distilled water under stirring (solution B). Then, solution A was added dropwise into solution B under vigorous stirring at room temperature. The weight percentage of silica added varied from 5 to 50% relative to TiO₂. The reaction solution was kept under stirring for 5 h and then aged at 25 °C for 24 h. Finally, the resulting gel was dried at 110 °C for 24 h, calcined at a certain temperature in air for 2 h with a heating rate of 5 °C/min, and labeled TS x–T, where x represented the theoretical molar percentage of silica in the catalyst and T indicated the calcination temperature (in the range of 350–750 °C).

3.3. Characterizations

TG/DSC analyses were performed in an air atmosphere with a heating rate of 10 °C/min from room temperature to 800 °C on a LABSYS evo instrument. X-ray diffraction patterns were recorded with a Rigaku Miniflex II X-ray diffractometer (Cu K α radiation, $\lambda = 0.154056$ nm). Crystallite size was estimated by applying the Debye-Scherrer equation to the (101) anatase peak. SEM analyses were performed on an ion beam scanning electron microscope (JEOL 6700F equipped with a field emission gun with an extract potential of 2.5 kV) combined with an EDX analyzer. The FT-IR spectra of the materials were recorded at room temperature in the wavelength range of 400 to 4000 cm⁻¹ with a Thermo Fisher Nicolet S10 spectrophotometer. Textural properties were obtained using an ASAP-2420 analyzer from Micromeritics. The specific surface area (S_{BET}) was calculated from the

Brunauer–Emmett–Teller (BET) equation from the physisorption of N₂ at 77 K. X-ray photoelectron spectroscopy (XPS) measurements were performed on an ultra-high vacuum (UVH) spectrometer equipped with a VSW Class WA hemispheric electron analyzer. The X-ray source used was a double Al K α X-ray (1486.6 eV) aluminum anode as incident radiation. The general high-resolution spectra were recorded in constant energy mode (100 and 20 eV, respectively). In order to correct for the shift in binding energy due to electrostatic charge, the internal reference used is the C1s peak at 284.9 eV, characteristic of sp² hybridized C. The background is subtracted according to the Shirley method.

3.4. Photocatalytic Measurement

First, 100 mg of the photocatalyst (0.5 g/L) was added to the sodium diclofenac solution (200 mL, 10 mg/L) in a 400 mL Pyrex beaker. The suspension was stirred in the dark for 30 min to reach the adsorption–desorption equilibrium. Then, the solution was irradiated with a low-power UV-A lamp (60 W/m², λ_{\max} = 368 nm). The distance between the light source and the suspension was 20 cm. At regular irradiation intervals, approximately 10 mL of suspension was taken with a syringe, then filtered with 0.22 μ m filters and analyzed by a UV-vis spectrophotometer of the brand ZUZI Spectrophotometer model 4211/50 at 276 nm, and the Total Organic Carbon concentration (TOC) was evaluated with a Shimadzu model TOC-L apparatus.

4. Conclusions

A simple sol-gel method was developed for the synthesis of anatase TiO₂/SiO₂ composites via surface reduction of Ti⁴⁺ ions to Ti³⁺ using rice husks as the source of the nanosilica. The results show that the biogenic silica increases the specific surface area of the materials and acts as good support that provides enough space for better dispersion of TiO₂ on the surface to avoid any possible agglomeration of the nanoparticles. The composites showed clear thermal stability and significant transformation of the anatase phase to rutile between 650 and 750 °C. In addition, the TiO₂/SiO₂ 20% composite showed anatase thermal stability up to 650 °C and excellent photocatalytic mineralization compared to P25 (83.68% after 2 h instead of 57.33% for P25).

Author Contributions: Conceptualization, D.R. and C.B.D.N.; methodology, C.B.D.N.; software, C.M.; validation, N.J.N., formal analysis, C.M.; investigation, C.B.D.N.; data curation, A.V.A.; writing—original draft preparation, C.B.D.N.; writing—review and editing, D.R.; supervision, D.R. and N.H.M.; Project administration, D.R.; funding acquisition, D.R. All authors have read and agreed to the published version of the manuscript.

Funding: This research was funded by Campus France “Eiffel” grant number 978617A.

Acknowledgments: The authors of this article would like to thank Campus France for the grant “Eiffel” awarded to Christian Brice DANTIO NGUELA.

Conflicts of Interest: The authors declare no conflict of interest.

References

1. Papageorgiou, M.; Kosma, C.; Lambropoulou, D. Seasonal occurrence, removal, mass loading and environmental risk assessment of 55 pharmaceuticals and personal care products in a municipal wastewater treatment plant in Central Greece. *Sci. Total Environ.* **2016**, *543*, 547–569. [[CrossRef](#)] [[PubMed](#)]
2. Zhang, Y.; Geißen, S.-U.; Gal, C. Carbamazepine and diclofenac: Removal in wastewater treatment plants and occurrence in water bodies. *Chemosphere* **2008**, *73*, 1151–1161. [[CrossRef](#)] [[PubMed](#)]
3. Pal, A.; Gin, K.Y.-H.; Lin, A.Y.-C.; Reinhard, M. Impacts of emerging organic contaminants on freshwater resources: Review of recent occurrences, sources, fate and effects. *Sci. Total Environ.* **2010**, *408*, 6062–6069. [[CrossRef](#)] [[PubMed](#)]
4. An, J.; Zhou, Q. Degradation of some typical pharmaceuticals and personal care products with copper-plating iron doped Cu₂O under visible light irradiation. *J. Environ. Sci.* **2012**, *24*, 827–833. [[CrossRef](#)]
5. Rosales, E.; Diaz, S.; Pazos, M.; Sanromán, M.A. Comprehensive strategy for the degradation of anti-inflammatory drug diclofenac by different advanced oxidation processes. *Sep. Purif. Technol.* **2019**, *208*, 130–141. [[CrossRef](#)]
6. Daghrir, R.; Drogui, P.; Robert, D. Modified TiO₂ for Environmental Photocatalytic Applications: A Review. *Ind. Eng. Chem. Res.* **2013**, *52*, 3581–3599. [[CrossRef](#)]

7. Nakata, K.; Fujishima, A. TiO₂ photocatalysis: Design and applications. *J. Photochem. Photobiol. C Photochem. Rev.* **2012**, *13*, 169–189. [[CrossRef](#)]
8. Wang, Y.; Su, Y.; Qiao, L.; Liu, L.; Su, Q.; Zhu, C.; Liu, X. Synthesis of one-dimensional TiO₂/V₂O₅ branched heterostructures and their visible light photocatalytic activity towards Rhodamine B. *Nanotechnology* **2011**, *22*, 225702. [[CrossRef](#)]
9. Lee, J.-W.; Kong, S.; Kim, W.-S.; Kim, J. Preparation and characterization of SiO₂/TiO₂ core-shell particles with controlled shell thickness. *Mater. Chem. Phys.* **2007**, *106*, 39–44. [[CrossRef](#)]
10. Wu, L.; Zhou, Y.; Nie, W.; Song, L.; Chen, P. Synthesis of highly monodispersed teardrop-shaped core-shell SiO₂/TiO₂ nanoparticles and their photocatalytic activities. *Appl. Surf. Sci.* **2015**, *351*, 320–326. [[CrossRef](#)]
11. Abega, A.V.; Ngomo, H.M.; Nongwe, I.; Mukaya, H.E.; Sone, P.-M.A.K.; Mbianda, X.Y. Easy and convenient synthesis of CNT/TiO₂ nanohybrid by in-surface oxidation of Ti³⁺ ions and application in the photocatalytic degradation of organic contaminants in water. *Synth. Met.* **2019**, *251*, 1–14. [[CrossRef](#)]
12. Kapridaki, C.; Pinho, L.; Mosquera, M.J.; Maravelaki-Kalaitzaki, P. Producing photoactive, transparent and hydrophobic SiO₂-crystalline TiO₂ nanocomposites at ambient conditions with application as self-cleaning coatings. *Appl. Catal. B Environ.* **2014**, *156–157*, 416–427. [[CrossRef](#)]
13. Wang, J.; Sun, S.; Ding, H.; Chen, W.; Liang, Y. Preparation of a composite photocatalyst with enhanced photocatalytic activity: Smaller TiO₂ carried on SiO₂ microsphere. *Appl. Surf. Sci.* **2019**, *493*, 146–156. [[CrossRef](#)]
14. Ren, C.; Qiu, W.; Chen, Y. Physicochemical properties and photocatalytic activity of the TiO₂/SiO₂ prepared by precipitation method. *Sep. Purif. Technol.* **2013**, *107*, 264–272. [[CrossRef](#)]
15. Tang, X.; Feng, Q.; Liu, K.; Tan, Y. Synthesis and characterization of a novel nanofibrous TiO₂/SiO₂ composite with enhanced photocatalytic activity. *Mater. Lett.* **2016**, *183*, 175–178. [[CrossRef](#)]
16. He, C.; Tian, B.; Zhang, J. Thermally stable SiO₂-doped mesoporous anatase TiO₂ with large surface area and excellent photocatalytic activity. *J. Colloid Interface Sci.* **2010**, *344*, 382–389. [[CrossRef](#)] [[PubMed](#)]
17. Yu, J.; Zhang, J.; He, J.; Liu, Z.; Yu, Z. Combinations of mild physical or chemical pretreatment with biological pretreatment for enzymatic hydrolysis of rice hull. *Bioresour. Technol.* **2009**, *100*, 903–908. [[CrossRef](#)]
18. Ndindeng, S.A.; Wopereis, M.; Sanyang, S.; Futakuchi, K. Evaluation of fan-assisted rice husk fuelled gasifier cookstoves for application in sub-Saharan Africa. *Renew. Energy* **2019**, *139*, 924–935. [[CrossRef](#)]
19. Alosaimi, E.H.; Alsohaimi, I.H.; Dahan, T.E.; Chen, Q.; Younes, A.A.; El-Gammal, B.; Melhi, S. Photocatalytic Degradation of Methylene Blue and Antibacterial Activity of Mesoporous TiO₂-SBA-15 Nanocomposite Based on Rice Husk. *Adsorpt. Sci. Technol.* **2021**, *2021*, 9290644. [[CrossRef](#)]
20. Efremova, S.V. Rice hull as a renewable raw material and its processing routes. *Russ. J. Gen. Chem.* **2012**, *82*, 999–1005. [[CrossRef](#)]
21. Sonobe, T.; Worasuwanarak, N. Kinetic analyses of biomass pyrolysis using the distributed activation energy model. *Fuel* **2008**, *87*, 414–421. [[CrossRef](#)]
22. Habeeb, G.A.; Mahmud, H.B. Study on properties of rice husk ash and its use as cement replacement material. *Mater. Res.* **2010**, *13*, 185–190. [[CrossRef](#)]
23. Hong, S.-S.; Lee, M.S.; Park, S.S.; Lee, G.-D. Synthesis of nanosized TiO₂/SiO₂ particles in the microemulsion and their photocatalytic activity on the decomposition of p-nitrophenol. *Catal. Today* **2003**, *87*, 99–105. [[CrossRef](#)]
24. Mahanta, U.; Khandelwal, M.; Deshpande, A.S. TiO₂@SiO₂ nanoparticles for methylene blue removal and photocatalytic degradation under natural sunlight and low-power UV light. *Appl. Surf. Sci.* **2022**, *576*, 151745. [[CrossRef](#)]
25. Kominami, H.; Yukishita, K.; Kimura, T.; Matsubara, M.; Hashimoto, K.; Kera, Y.; Ohtani, B. Direct Sol-vothermal Formation of Nanocrystalline TiO₂ on Porous SiO₂ Adsorbent and Photocatalytic Removal of Nitrogen Oxides in Air over TiO₂-SiO₂ Composites. *Top. Catal.* **2008**, *47*, 155–161. [[CrossRef](#)]
26. Yang, Z.-Y.; Shen, G.-Y.; He, Y.-P.; Liu, X.-X.; Yang, S.-J. Preparation of TiO₂/SiO₂ composite oxide and its photocatalytic degradation of rhodamine B. *J. Porous Mater.* **2016**, *23*, 589–599. [[CrossRef](#)]
27. Siddiq, A.; Sabir, S.; Hussain, S.T.; Muhammad, B. Highly active mesoporous SiO₂-TiO₂ based nanocomposites for photocatalytic degradation of textile dyes and phenol. *Eur. J. Chem.* **2013**, *4*, 388–395. [[CrossRef](#)]
28. Florez, D.M.M.G.; Ale, R.B.G.; Idme, A.F.H.; Alarcon, L.A.L.; Huallpa, E.A.; Castro, Y.; Apestegui, P.G.R.; Rodriguez, J.M.R. SiO₂-TiO₂ Films Supported on Ignimbrite by Spray Coating for the Photocatalytic Degradation of NO_x Gas and Methyl Orange Dye. *Int. J. Photoenergy* **2020**, *2020*, 4756952. [[CrossRef](#)]
29. Cheng, J.; Zhao, L.; Li, G.; Li, F.; Yao, M. B/Co/Fe tridoped TiO₂/SiO₂ composite films for improved photocatalytic degradation of organic pollutants under visible light. *Inorg. Chem. Commun.* **2020**, *119*, 108089. [[CrossRef](#)]
30. Yener, H.B.; Helvacı, Ş.Ş. Effect of synthesis temperature on the structural properties and photocatalytic activity of TiO₂/SiO₂ composites synthesized using rice husk ash as a SiO₂ source. *Sep. Purif. Technol.* **2015**, *140*, 84–93. [[CrossRef](#)]
31. Huang, C.; Bai, H.; Huang, Y.; Liu, S.; Yen, S.; Tseng, Y. Synthesis of Neutral SiO₂/TiO₂ Hydrosol and Its Application as Antireflective Self-Cleaning Thin Film. *Int. J. Photoenergy* **2012**, *2012*, 620764. [[CrossRef](#)]
32. Hoffmann, M.R.; Martin, S.T.; Choi, W.; Bahnemann, D.W. Environmental Applications of Semiconductor Photocatalysis. *Chem. Rev.* **1995**, *95*, 69–96. [[CrossRef](#)]